Proc. Natl. Acad. Sci. USA
Vol. 92, pp. 9210–9214, September 1995
Biophysics

Mixing of connexins in gap junction membrane channels

(intercellular communication/electron microscopy/image analysis/connexon structure/molecular mass determination)

GINA SOSINSKY*

Rosenstiel Basic Medical Sciences Research Center, Brandeis University, Waltham, MA 02254-9110

Communicated by Donald L. D. Caspar, Florida State University, Tallahassee, FL, May 19, 1995 (received for review July 7, 1994)

ABSTRACT **Gap junctions are plaque-like clusters of intercellular channels that mediate intercellular communication. Each of two adjoining cells contains a connexon unit which makes up half of the whole channel. Gap junction channels are formed from a multigene family of proteins called connexins, and different connexins may be coexpressed by a single cell type and found within the same plaque. Rodent gap junctions contain two proteins, connexins 32 and 26. Use of a scanning transmission electron microscope for mass analysis of rodent gap junction plaques and split gap junctions provided evidence consistent with a model in which the channels may be made from (*i*) solely connexin 26, (*ii*) solely connexin 32, or (*iii*) mixtures of connexin 26 and connexin 32 in which the two connexons are made entirely of connexin 26 and connexin 32. The different types of channels segregate into distinct domains, implying that connexon channels self-associate to give a nonrandom distribution within tissues. Since each connexin confers distinct physiological properties on its membrane channels, these results imply that the physiological properties of channels can be tailored by mixing the constituent proteins within these macromolecular structures.**

Direct intercellular communication is mediated by membrane channel structures called gap junctions† (1). These intercellular channels regulate cell metabolism (2), differentiation (3), and the transmission of electrical impulses (4). Each cell contributes half of the intercellular channel, an oligomeric assembly of integral membrane proteins called a connexon (ref. 5 and Fig. 1). Connexins, a family of related proteins with a common folding topology, are the constituent proteins of the connexon (6).

Different connexins may be present within a given cell type. Rodent hepatocyte gap junctions contain both connexin 32 (Cx32) and connexin 26 (Cx26). Cx26, consisting of 226 aa, is the smallest of the gap junction protein family, whereas Cx32 contains 272 aa. Mouse liver gap junction preparations contain Cx32 and Cx26 in a molar ratio of ≈2:1, while in rat liver preparations the ratio of Cx32 to Cx26 (7) is ≈10:1. In guinea pig liver the majority of the protein is Cx26 (8). Connexins 26 and 32 colocalize both *in situ* and in isolated gap junction plaques (7, 9). Functional heterotypic junctions are obtained when the mRNAs for Cx32 and Cx26 are expressed in paired *Xenopus* oocytes (10). Competition experiments involving coinjection of Cx32 and Cx26 mRNAs in *Xenopus* oocytes show that heterotypic junctions of Cx32 and Cx26 form with equal probability to homotypic junctions (11). However, it is not known whether heterotypic connexon pairs occur *in vivo*, and these physiological studies cannot discern mixtures of connexins within connexons.

These observations raise the possibility that naturally occurring gap junction channels could be formed from more than one type of connexin. The mixed channels may have distinct physiological roles, since homotypic junctions have distinctive voltage gating properties which depend on the constituent connexins. Three possibilities for the associations of Cx26 and Cx32 within connexons are that (*i*) each gap junction channel is made from only one type of connexin (homotypic channels), (*ii*) individual gap junction connexons are made from only one type of connexin but connexons made from different connexins associate with each other (heterotypic channels), and (*iii*) gap junction channels are made from random mixtures of connexins (heteromeric channels). Populations of connexons in which the connexins associate according to these three possibilities are predicted to have different mass distributions (Fig. 2). By applying image analysis methods to micrographs obtained from a STEM, it is possible to identify individual connexons in a gap junction plaque and determine their masses. Here I describe an application of STEM mass analysis (12) to isolated gap junction membranes to determine the protein composition of the connexon units and the distribution of different connexins within gap junction connexon arrays.

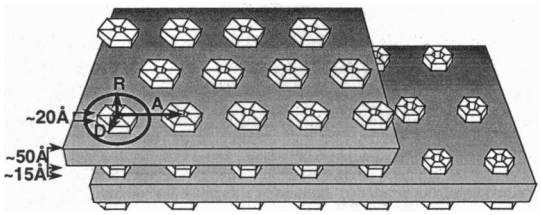

FIG. 1. Illustration of the gap junction lattice and measurements made on scanning transmission electron microscope (STEM) images. Each connexon is drawn as a hexamer of connexin subunits. Vector **A** is the lattice constant. Vector **D** is the outer radius of the connexon, ≈34 Å. The measurements shown in the histograms of Figs. 5 and 6 are the total mass within the circle of radius *R*.

MATERIALS AND METHODS

Isolation of Gap Junctions. Mouse and rat liver gap junctions were prepared by the method of Fallon and Goodenough (13). This protocol produces gap junction plaques that are more crystalline than plaques obtained with the protocol devised by Hertzberg (14). There was no possibility of subunit exchange because the membranes were never solubilized. Single layers of connexons (split junctions) of these same samples were prepared by treatment with 4 M urea at pH 8 (15).

Gel Electrophoresis. SDS/polyacrylamide gels and immunoblots were prepared according to Francis *et al.* (16). The

The publication costs of this article were defrayed in part by page charge payment. This article must therefore be hereby marked "*advertisement*" in accordance with 18 U.S.C. §1734 solely to indicate this fact.

Abbreviations: Cx26 and Cx32, connexins 26 and 32; STEM, scanning transmission electron microscope.

*Present address: Department of Biology 0322, University of California, San Diego, 9500 Gilman Drive, La Jolla, CA 92093-0322.

†Nomenclature: a connexon is the oligomer of the protein connexin, and two connexons pair to make up a gap junction channel (also referred to as an intercellular channel). If a connexon is composed of only one connexin isoform, it is referred to as homomeric; if it is composed of more than one connexin isoform, it is heteromeric. A homotypic junction can only occur if two homomeric connexons pair; a heterotypic junction may be composed of either two different homomeric connexons or two heteromeric connexons.

anti-Cx32 antibody (17) and the anti-Cx26 antibody (18) have been described. Densitometry was performed on an E-C Apparatus densitometer.

Electron Microscopy. Specimens imaged with conventional electron microscopy were stained with 2% uranyl acetate and examined on a Philips 301 electron microscope. Samples were prepared for the Brookhaven STEM and images were recorded as described by Sosinsky *et al.* (19).

Modeling of Connexon Populations. The curves shown in Fig. 2 were calculated from the protein part of the assembly by assuming that the connexon is a hexamer and that the overall composition is 2:1 in Cx32 and Cx26. Errors were modeled by convolving the ideal distributions with Gaussian distributions with standard deviation σ. Population distributions for the case in which there were random mixtures of connexins in each connexon were modeled by using a random number generator to sample the various possible combinations.

Image Analysis. Images were chosen for correlation analysis only when the calculated diffraction patterns showed diffraction spots characteristic of hexagonal lattices and the lattice constants were within range of previously observed lattice parameters (20). The [1, 0] and [0, 1] vectors and relative orientation to a horizontal axis were measured from the calculated diffraction pattern. Correlation analysis methods for identifying the connexon-pair centers (21, 22) were applied by rotating a reference image containing an arrangement of a central connexon plus its six neighbors by the measured orientation angle and cross-correlating the reference with the boxed and floated STEM image. Peak maps identifying the positions of the connexon centers were calculated from the cross-correlation maps. For the images that contained more than one lattice domain, cross-correlation maps were calculated for each domain. Peak maps were cut and spliced together in order to calculate coordinates for connexons or connexon pairs.

Mass Determinations. Coordinates for the connexon centers were put into the mass calculation program and the pixel intensities were integrated over a radius of 37 Å (see Fig. 1). Each pixel in the digital STEM image corresponds to 10 Å. Background measurements were made for each image by boxing areas of carbon film around the membranes. For each image, the background value was typically the average of two to four boxed areas of carbon film around the membrane. The standard deviation of this background value within each image was usually <4% of the average background, suggesting that the local carbon film thickness was uniform. Tobacco mosaic virus (TMV) was included as a mass standard. TMV scale factors are usually accurate to better than 5% (12). Each experimentally determined TMV scale factor was plotted against the average background for the image. A line was fit by a least-squares algorithm to obtain a relationship for converting measured masses to absolute mass values. As an additional scale factor, mass-per-area measurements were also made for purple membrane samples.

Mass measurements were obtained from large numbers of channels (>1000 measurements for gap junction plaques and 100–300 measurements for single connexon layers). Images that are color-coded according to the values of the observed masses (see Fig. 5) were calculated in a one-to-one correspondence with the original image to show the mass distribution of the connexons within the membrane plaque.

RESULTS

Protein Composition of Mouse and Rat Gap Junction Samples. As judged by SDS/PAGE and densitometry (Fig. 3), the connexin composition of the rat liver plaques was ≈1:10 in Cx26 and Cx32. In mouse liver gap junctions the proportion of Cx26 to Cx32 was ≈1:2. The presence of these proteins was further verified by immunoblotting (Fig. 3). The complicated

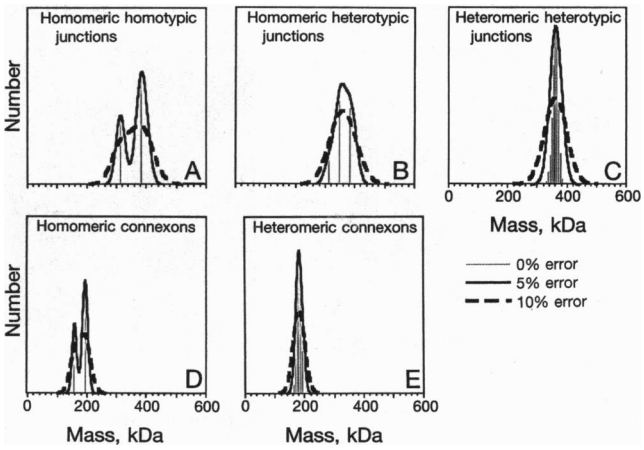

FIG. 2. Calculated mass distributions for mouse gap junction plaques. Model connexon mass distributions were calculated in order to interpret the experimentally determined histograms from individual images. Solid lines indicate curves broadened by standard deviations (simulated errors) of 5% of the mean mass; dashed lines indicate errors of 10% of the mean; and dotted lines are the positions of the peaks without measurement errors. *A–C* are calculated for whole membrane channels, whereas *D* and *E* are calculated for connexons. (*A*) Two populations of homomeric homotypic junctions, (*B*) Three combinations are possible: two types of homotypic junction and one heterotypic junction. (*C*) Random mixtures of Cx32 and Cx26 in both connexons (14 possible combinations). (*D*) Two populations of homomeric connexons. (*E*) Random mixtures of 7 possible combinations of two connexin isoforms. These simulations show that for two populations of homotypic junctions which are different in mass by 20% of the mean, the percentage error must be ≈5% of the average masses in order for the two mass maxima to be resolved.

banding pattern of the Cx32 immunoblot of the rat liver gap junction sample is due to proteolytic products of Cx32 and their oligomers. The immunoblot reaction enhances all protein products containing the epitopes. Since the detection reaction used is enzymatic (horseradish peroxidase; see ref. 16), the blots are not quantitative. The protein composition is more quantitatively measured by Coomassie staining than by immunoblotting. The SDS/PAGE banding pattern of the split junction samples was the same as for the intact junctions, indicating the same relative proportions of Cx26 and Cx32.

Quantitative Analysis of STEM Images of Intact Gap Junctions. STEM images of mouse and rat liver gap junctions (Fig. 4) do not show as high-resolution diffraction patterns as low-irradiation negatively stained or frozen-hydrated TEM images, but the connexons were comparably packed within a hexagonal lattice (see diffraction patterns in Fig. 4). Cracks in the membranes, particularly evident in the rat liver preparations, were due to freeze drying of samples for collection of STEM data.

For the images obtained in this study, the lattice constants for individual domains ranged from 80.2 ± 2.8 Å (n = 74) for the mouse liver gap junction preparation to 83.9 ± 3.0 Å (n = 44), 80.9 ± 3.1 Å (n = 29), and 86.6 ± 3.5 Å (n = 8) for three separate preparations of rat liver junction. Lattice constants for single-layer connexon lattices were smaller, 77.5 ± 2.1 Å (n = 7) for single mouse layers derived from the mouse gap junction sample and 80.4 ± 4.0 Å (n = 24) obtained from the first rat liver gap junction sample.

Because of the low contrast in the STEM images, the connexon boundary was not discernible. The observed mass distributions shown in Figs. 5 and 6 are higher than the expected mass distributions shown in Fig. 2 because the experimentally measured area of 4500 Å^2 includes lipids as well as the connexon (or connexon pair).

A comparison of the average gap junction channel masses obtained from each of the 44 mouse liver gap junction images

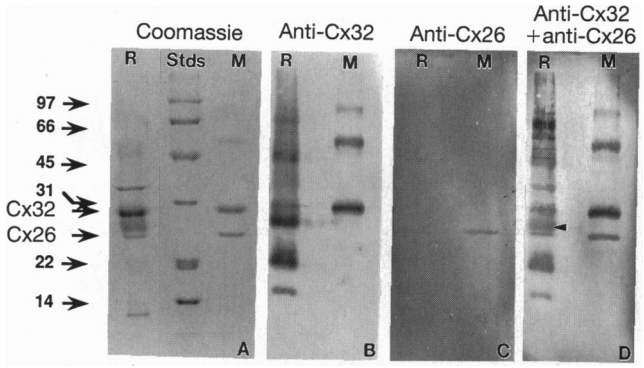

FIG. 3. Protein composition. (*A*) As judged by SDS/PAGE followed by Coomassie blue staining, the connexin composition in rat liver plaques (lane R) is ≈1:10 in Cx26 and Cx32. In mouse liver gap junctions (lane M) the Cx26/Cx32 ratio is ≈1:2. Molecular masses (kDa) of standard proteins (Stds) are at left. (*B–D*) The presence of Cx26 and Cx32 was verified by immunoblotting with two antibodies, one specific for Cx32 (*B*) and one which recognizes Cx26 (*C*). The anti-32 immunoblot in *B* was then blotted with the anti-26 antibody to show the nonoverlap of the two bands (*D*). Arrowhead in *D* indicates the presence of proteolyzed Cx32, which runs slightly slower than Cx26, in the rat preparation. No proteolysis products were found in the mouse preparation. The higher molecular weight species in the anti-Cx32 Western blots are aggregates of Cx32.

and the 28 rat liver gap junction images revealed skewed average mass distributions for both mouse and rat samples (data not shown). However, the mass averages in the mouse data set are skewed toward higher masses, while the distribution of rat averages are skewed toward lower masses. This skewing reflects the expected difference in the relative proportions of Cx26 in the two samples. The lower observed masses of the rat specimens may be due to proteolysis of Cx32.

In the mouse liver specimens (where the Cx26/Cx32 ratio was 1:2), 4 images from a data set of 44 gave bimodal distributions of connexon masses. In these cases, the separation between the two mass maxima was about 20% of the total mass. Therefore, these bimodal mass distributions are consistent with populations containing homotypic channels which consist solely of Cx26 and Cx32 (with expected protein masses of 312 and 384 kDa). Fits to these bimodal histograms were performed by the Marquardt–Leverberg method (23) with a two-Gaussian function with variable positions, widths, and peak heights. These fits gave standard deviations for the Gaussians which were 5–6% of the mean values, which can be taken as a measure of the noise in the connexon mass determinations. When these 4 images were displayed in color, a segregation of channels with different masses became apparent (Fig. 5 *Top*). A difference image between correlation averages from "heavy" and "light" mouse membrane channels in the image presented in Fig. 5*A* appears to show some structure in the connexon region. The difference image is not uniform as would be the case if part of the plaques were underlaid by some contaminating material (data not shown). Mass-per-unit-cell measurements in areas of the image containing mainly Cx32 and areas containing mainly Cx26 were consistent with expectations based on the protein and lipid composition obtained by x-ray analysis (5). Thus, the homotypic channels appear to self-associate into separate domains.

The other 40 images in the mouse liver data set gave unimodal distributions of connexon masses. In some of these plaques the rms value of the mass distribution was only ≈5% of the mean mass (Fig. 5 *Middle*). Plaques which give unimodal mass distributions with small standard deviations are most likely to contain connexons consisting of only a single type of connexin. Therefore, these mass distributions were interpreted as containing a single population of either Cx26 or Cx32, depending on the average mass of the population.

The mass distribution from a population of connexons containing heterotypic junctions of Cx26 and Cx32 in stoichometric quantities should broaden to give rms values of ≈9% of the mean (see Fig. 2*B*). Therefore, plaques which give a broader (rms variation > 8% of the mean) unimodal distribution of masses may be accounted for by connexons which contain mixtures of Cx26 and Cx32 (Fig. 5 *Bottom*). However, in the presence of expected errors in the connexon mass determinations, curves with the same general appearance could be obtained for junctions made from mixtures of either connexons of single connexin types or gap junctions in which the connexins were randomly assembled (Fig. 2 *B* and *C*).

As an experimental control on the reliability of these histograms, a similar analysis of rat liver junction plaques (which contain primarily Cx32) was carried out. Only 1 image from a data set of 28 images had a bimodal appearance. In this case, the smaller peak occurred at a lower mass value, indicating a small proportion of Cx26 homotypic junctions. Thus, the analysis of the rat junction data is consistent with the large preponderance (10:1) of Cx32 and Cx26.

Using the equation of Wall and Hainfeld (24), the error in mass measurements of individual gap junction membrane channels is ≈7% of the mean mass. Given the inverse relationship between mass and accuracy, relative errors in measurements for hemichannels should be slightly larger. As a test of the accuracy of the measurements, a portion of the carbon film (which should have no periodic structure) was cross-correlated with an arbitrary connexon reference image. The average standard deviation for mass distributions from 20 images of carbon films was 4.0 ± 0.7% of the mean. For 15 images of membranes which did not contain hexagonal diffraction patterns, the average standard deviation for those

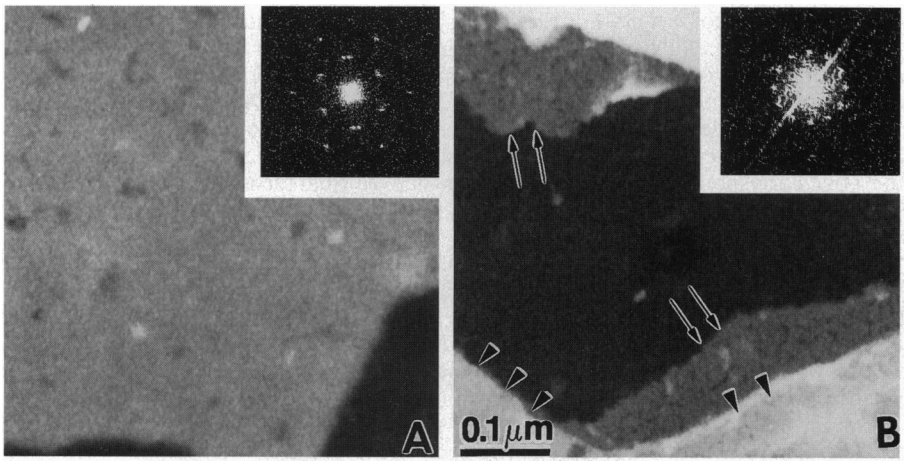

FIG. 4. Gap junction images. STEM micrographs of freeze-dried mouse gap junctions (*A*) and split junctions (single layers of connexons) (*B*). The connexons are held within a hexagonal lattice as indicated by their diffraction patterns (*Insets*). In *B*, arrows point to single connexon membranes and arrowheads point to double membrane layers.

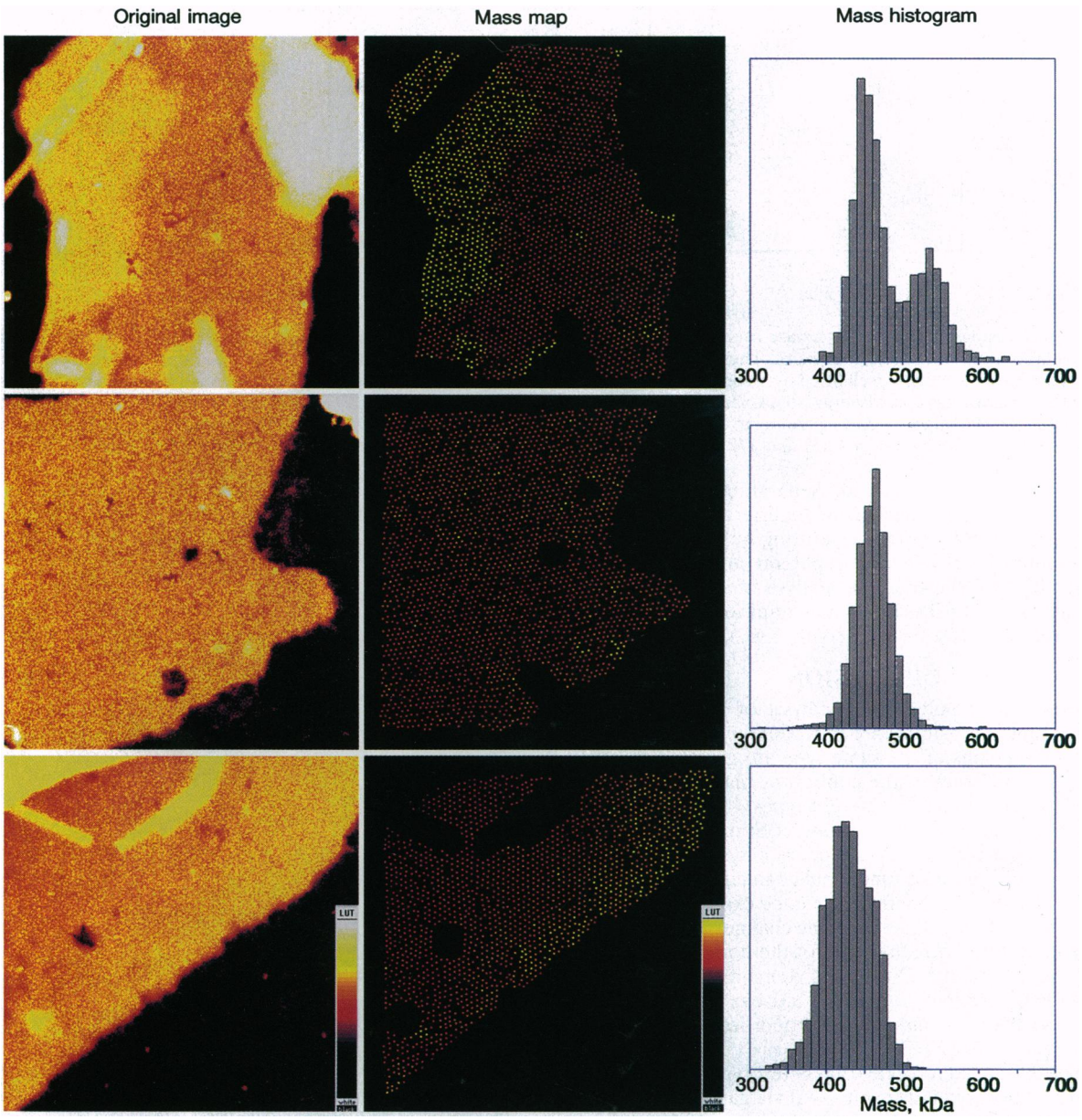

FIG. 5. Mouse gap junction STEM images, mass maps, and histograms. Computed connexon masses are displayed on a 1- to 600-kDa color table to show the distribution of connexon masses within the individual micrographs of mouse gap junctions. These "mass maps" (*Center*, color table is displayed as an *Inset* in *Bottom*) are helpful in interpreting the histograms (*Right*) and checking the analysis against the original images (*Left*). The micrographs are displayed on an expanded color table but represent pixel intensities of 0–255 (color table is displayed as an *Inset* in *Bottom Left*). In a small number of images in the mouse liver preparation, the histograms were bimodal with a separation between peaks that was ≈20% of the average mass (*Top*). In these cases, the high and low mass junctions segregate into distinct domains. While most of the mouse images gave unimodal mass distributions, the width and positions of the mass maxima varied. In the mouse preparations many images gave sharp mass distributions (*Middle*) whereas other images gave broader unimodal distributions (*Bottom*).

histograms was 5.9 ± 0.7% of the mean. These measurements reflect the intrinsic error in measurement.

Analysis of Split Junction Images. In the analysis of the whole junctions, the broad unimodal histograms could be explained by either heterotypic homomeric membrane channels or by two paired heteromeric connexons. To decide between these two possibilities, mass distributions for connexons in urea-split plaques of mouse junctions were obtained. In both the rat and mouse data sets, the average masses obtained from split junctions were always half of the masses obtained from intact junctions. This reflects an internal consistency of the absolute scaling of the whole- and split-junction data sets. A peak-fitting analysis of histograms of single connexons reveals bimodal mass distributions in three of five images (Fig. 6*A*) and unimodal distributions (rms value ≈ 9% of the average value) in the other two images (Fig. 6*B*). When masses from all five images are combined, the total population appears bimodal (Fig. 6*C*). The ratio of the peak heights of these Gaussians is consistent with the ≈2:1 ratio of Cx32 to Cx26 obtained from the densitometry of the gel bands in Fig. 3. The average masses used in the curve fitting were 10% higher than the calculated protein mass because the measured masses contained some lipids. In Fig. 6, these masses corresponded to 211 kDa for homomeric Cx32 connexons and 172 kDa for homomeric Cx26 connexons. A third Gaussian, corresponding to a putative population of heteromeric connexons, was also included in the histogram fitting. The magnitude of this third Gaussian was either within the estimated errors of the analysis or vanished in the analysis. The histograms in Fig. 6*A* and *C* contain a tail at high masses which may reflect some

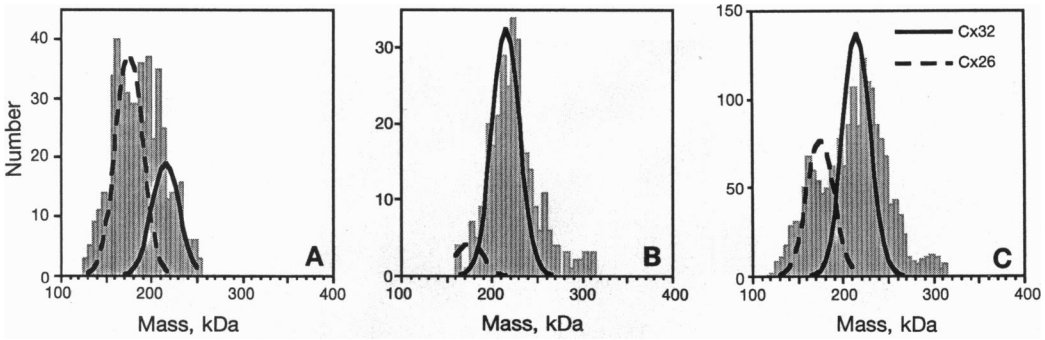

FIG. 6. Mass histograms from split mouse liver gap junctions. (*A*) Mass histogram obtained from split mouse gap junctions that is well fitted by two populations of homomeric connexons. These two populations are modeled by curves with Gaussian error distributions. (*B*) Example of a connexon mass histogram that is well fitted by a single Gaussian model for a single type of connexon. This is essentially a unimodal mass distribution of Cx32 with no significant contribution from Cx26. (*C*) Histogram of the pooled connexon masses. This histogram appears bimodal and is fitted by two populations of connexons corresponding to Cx32 and Cx26. The standard deviations for the fitted Gaussians shown were chosen to be ≈7% of the average masses (211 kDa for Cx32 and 172 kDa for Cx26). This standard deviation was used to illustrate the physical model in Fig. 2.

unexplained adhering mass. Peak separations slightly larger than the expected values may be due to differences in adhering lipids or residual urea from the splitting buffer. Mass histograms obtained from images of split rat junctions were all unimodal (data not shown). This analysis of the split junction plaques indicates that the individual connexons in these samples are made of solely Cx26 or solely Cx32.

DISCUSSION

Summary. The results from analysis of whole and split mouse gap junction plaques are consistent with the interpretation that connexins of the same type are grouped together into connexons. However, the connexons may pair with connexons of either similar or different types.

Implications for Functional Channel States. Physiological studies with the *Xenopus* oocyte expression system have shown that it is possible to make functional channels from different connexins (25, 26). Cx32 and Cx26 can be expressed in paired *Xenopus* oocytes to create heterotypic channels with a voltage profile shaped differently than that of the homotypic pairings (10). Shortening of the C-terminal domain of Cx43 to the length of the C-terminal domain in Cx32 changes the channel properties so that its conductance properties resemble Cx32 homotypic junctions (27).

Evidence exists that indicates that heterotypic junctions may exist *in vivo*. Lucifer yellow dye passed via gap junctions from astrocytes (containing Cx32) to oligodendrocytes (containing Cx43) and Müller cells, but rarely transferred in the opposite direction (28). In addition, Cx32 has been shown to be expressed in all parts of rat liver, whereas Cx26 is differentially expressed in periportal regions (9). An analysis of confocal microscopy images of rat epidermis shows domains of segregated Cx43 and segregated Cx26 as well as regions of overlap of the two connexins (29). However, due to the limitations of these techniques, plaques containing interspersed homotypic channels cannot be differentiated from plaques containing heterotypic junctions. The resolution provided by the STEM is much greater and allows for single-connexon mass measurements. The measurements presented here show that segregation of homotypic junctions occurs and that mixtures of the connexin proteins in whole channels are primarily due to pairings of different homomeric connexons.

These findings open the possibility that intercellular channels are tailored to suit the physiological needs of the cells by varying the connexin composition of the channel. The STEM mass analysis presented here provides evidence that three types of channel made from Cx26 and Cx32 form *in vivo*, with different types of channels segregating into distinct domains, perhaps reflecting their original spatial tissue organization.

I thank D. Goodenough and D. Paul for antibodies; J. Wall, M. Simon, and B. Yu-Lin for data collection at the Brookhaven National Laboratory STEM Facility; and M. Craig for photographic work. Discussions with D. Goodenough, L. Makowski, N. Francis, and J. Badger are gratefully acknowledged. This work was started under National Institutes of Health Grant CA47439 to D. L. D. Caspar and was expanded and completed under Grant GM43217 to G.S.

1. Bennett, M. V. L. & Goodenough, D. A. (1978) *Neurosci. Res. Program Bull.* **16,** 375–486.
2. Hooper, M. L. & Subak-Sharpe, J. H. (1981) *Int. Rev. Cytol.* **69,** 45–104.
3. Gilula, N. B., Reeves, O. R. & Steinbach, A. (1972) *Nature (London)* **235,** 262–265.
4. Fraser, S. E., Green, C. R., Bode, H. R. & Gilula, N. B. (1987) *Science* **237,** 49–55.
5. Makowski, L., Caspar, D. L. D., Phillips, W. C. & Goodenough, D. A. (1977) *J. Cell Biol.* **74,** 629–645.
6. Beyer, E. C., Paul, D. L. & Goodenough, D. A. (1990) *J. Membr. Biol.* **116,** 187–194.
7. Zhang, J.-T. & Nicholson, B. J. (1989) *J. Cell Biol.* **109,** 3391–3401.
8. Kuraoka, A., Iida, H., Hatae, T., Shibata, Y., Itoh, M. & Kurita, T. (1993) *J. Histochem. Cytochem.* **41,** 971–980.
9. Traub, O., Look, J., Dermietzel, R., Brümmer, F., Hülser, D. & Willecke, K. (1989) *J. Cell Biol.* **108,** 1039–1051.
10. Barrio, L. C., Suchyna, T., Bargiello, T., Xu, L. X., Roginski, R. S., Bennett, M. V. L. & Nicholson, B. J. (1991) *Proc. Natl. Acad. Sci. USA* **88,** 8410–8414.
11. Nicholson, B. J., Suchyna, T., Xu, L. X., Hammernick, P., Cao, F. L., Fourtner, C., Barrio, L. & Bennett, M. V. L. (1993) *Prog. Cell Res.* **3,** 3–14.
12. Wall, J. S. & Hainfeld, J. (1986) *Annu. Rev. Biophys. Biophys. Chem.* **15,** 355–376.
13. Fallon, R. F. & Goodenough, D. A. (1981) *J. Cell Biol.* **90,** 521–526.
14. Hertzberg, E. L. (1984) *J. Biol. Chem.* **254,** 2138–2147.
15. Ghoshroy, S., Goodenough, D. A. & Sosinsky, G. E. (1995) *J. Membr. Biol.* **146,** 15–28.
16. Francis, N. R., Irikura, V. M., Yamaguichi, S., DeRosier, D. J. & Macnab, R. M. (1992) *Proc. Natl. Acad. Sci. USA* **89,** 6304–6308.
17. Goodenough, D. A., Paul, D. L. & Jesaitis, L. (1988) *J. Cell Biol.* **107,** 1817–1824.
18. Goliger, J. A. & Paul, D. L. (1994) *Dev. Dyn.* **200,** 1–13.
19. Sosinsky, G. E., Francis, N. R., DeRosier, D. J., Wall, J. S., Simon, M. N. & Hainfeld, J. (1992) *Proc. Natl. Acad. Sci. USA* **89,** 4801–4805.
20. Makowski, L., Caspar, D. L. D., Phillips, W. C., Baker, T. S. & Goodenough, D. A. (1984) *Biophys. J.* **45,** 208–218.
21. Saxton, W. O. & Baumeister, W. (1982) *J. Microsc.* **127,** 127–138.
22. Sosinsky, G. E., Baker, T. S., Caspar, D. L. D. & Goodenough, D. A. (1990) *Biophys. J.* **58,** 1213–1226.
23. Press, W. H., Flannery, B. P., Teukolsky, S. A. & Vetterling, W. T., (1986) *Numerical Recipes* (Cambridge Univ. Pres, Cambridge, U.K.).
24. Wall, J. S. & Hainfeld, J. P. (1984) in *Proceedings of the 42nd Electron Microscopy Society of America Annual Meeting*, ed. Bailey, G. W. (San Francisco Press, San Francisco), pp. 154–157.
25. Swenson, K. I., Jordan, J. R., Beyer, E. C. & Paul, D. L. (1989) *Cell* **57,** 145–155.
26. Dahl, G., Miller, T., Paul, D., Voellmy, R. & Werner, R. (1987) *Science* **236,** 1290–1293.
27. Liu, S., Taffet, S., Stoner, L., Delmar, M., Vallano, M. L. & Jalife, J. (1993) *Biophys. J.* **64,** 1422–1433.
28. Robinson, S. R., Hampson, E. C. G. M., Munro, M. N. & Vaney, D. I. (1993) *Science* **262,** 1072–1074.
29. Risek, B., Klier, F. G. & Gilula, N. B. (1994) *Dev. Biol.* **164,** 183–196.